Formation, Detection, and Characterization of Extrasolar Habitable Planets
Proceedings IAU Symposium No. 293, 2012
N. Haghighipour, ed.

doi:10.1017/S1743921313012933

Laminar Accretion in the Habitable Zone of Protoplanetary Disks

Xue-Ning Bai[1,2] and James M. Stone[1]

[1]Department of Astrophysical Sciences, Peyton Hall, Princeton, NJ 08540, USA

[2]Current Address: Institute for Theory and Computation, Harvard-Smithsonian Center for Astrophysics, 60 Garden Street, MS-51, Cambridge, MA 02138
email: xbai@cfa.harvard.edu

Abstract. Protoplanetary disks (PPDs) are widely believed to be turbulent as a result of the magnetorotational instability (MRI). We perform magnetohydrodynamical simulations of PPDs that for the first time, take into account both Ohmic resistivity and ambipolar diffusion in a self-consistent manner. We show that in the inner region of PPDs that corresponds the habitable zone, the MRI is completely suppressed due to the interplay between magnetic field and ambipolar diffusion. The gas in this region is laminar throughout the entire vertical extent of the disk. Instead of MRI-driven accretion, a strong magnetocentrifugal wind is launched that efficiently carries away disk angular momentum. A physical wind geometry requires the presence of a strong current layer that is offset from the disk midplane where horizontal magnetic fields flip. We show that the entire accretion flow proceeds through this strong current layer. The non-turbulent nature of the gas flow strongly favors the habitable zone as the site for planetesimal formation, and has important implications for their subsequent growth into terrestrial planets.

Keywords. protoplanetary disks, magnetorotational instability, magnetocentrifugal winds

1. Introduction

Protoplanetary disks (PPDs) are typically found to be actively accreting onto the central protostar with accretion rate of the order $10^{-8} M_\odot$ yr^{-1} (Hartmann *et al.* 1998). Meanwhile, outflow is ubiquitously found from young stellar objects, with typical rate of mass outflow of the order 10% of the accretion rate (Hartigan *et al.* 1995). Despite the large number of observational programs aiming at revealing the structure, composition and evolution of PPDs, two crucial questions on the gas dynamics of PPDs remain poorly understood: What is the level of turbulence in PPDs? What drives the accretion and outflow in PPDs? It is almost certain that magnetic fields play a crucial role in these processes, mainly via two mechanisms: the magnetorotational instability (MRI, Balbus & Hawley, 1991) and the magnetocentrifugal wind (MCW, Blandford & Payne, 1982).

The MRI states that conducting gas in differentially rotating disks threaded by a weak magnetic field is linearly unstable, which generates turbulence and transports angular momentum outward to drive disk accretion. The MRI requires the gas to be sufficiently ionized to be well coupled with the magnetic field. However, PPDs are extremely weakly ionized, which introduces strong non-ideal magnetohydrodynamic (MHD) effects (e.g., Bai, 2011a) including Ohmic resistivity, the Hall effect, and ambipolar diffusion (AD). The effect of Ohmic resistivity has been thoroughly explored both semi-analytically and numerically (e.g., Fleming & Stone, 2003, Ilgner & Nelson, 2006, Bai & Goodman, 2009, Okuzumi & Hirose, 2011), which all conform to the conventional framework of layered accretion in the inner region of PPDs (Gammie, 1996): in the inner disk, accretion proceeds in the MRI-active layer in the disk surface whereas the midplane region is too resistive

for the MRI to operate (i.e., the dead zone). However, other non-ideal MHD effects, in particular AD which plays a dominant role at disk surface, are largely ignored.

The linear behavior of the MRI in the presence of the Hall effect (e.g., Pandey & Wardle, 2012) and AD is relatively well understood (e.g., Kunz & Balbus, 2004). In the non-linear regime, it was found that the Hall effect probably does not affect the saturation level of the MRI by much (Sano & Stone, 2002), while for the MRI to operate in the AD dominated regime, the magnetic field has to be sufficiently weak (Bai & Stone, 2011). Applying these criteria to PPDs, Bai (2011a) found that the MRI-driven accretion rate in the inner region of PPDs is at least one order of magnitude smaller than the observed rates, which is largely due to the effect of AD. In the outer disk, Bai (2011b) showed that the presence of tiny polycyclic aromatic hydrocarbons promotes accretion due to a net reduction of AD, where the MRI-driven accretion rate can achieve the observed rates.

The MCW scenario states that outflowing gas from the disk can be centrifugally accelerated along open magnetic field lines as long as the field lines are inclined relative to disk normal by more than 30° (for Keplerian disks). The MCW extracts angular momentum vertically from the disk which very efficiently drives accretion. A prerequisite for the MCW mechanism is that the gas must flow out from the disk at first place. Such wind launching or mass loading problem requires detailed modeling of disk microphysics (e.g., the MRI turbulence and non-ideal MHD effects), which was not properly reflected in most global wind simulations. It is generally believed that relatively strong vertical magnetic field of the order equipartition strength at disk midplane is needed to launch the MCW (Wardle & Koenigl, 1993, Ferreira & Pelletier, 1995, Königl *et al.*, 2010), which is too strong for the MRI to operate. However, such strong vertical field would drive very strong outflow which rapidly depletes the disk, leading to a thin disk with very low surface density (Combet & Ferreira, 2008).

In this work, we present the most realistic MHD simulations to date for the inner region of PPDs which simultaneously takes into account Ohmic resistivity and AD and show that the MRI is completely suppressed even in the presence of a very weak vertical field, and angular momentum transport is carried by a laminar MCW.

2. 3D Simulations: the Dramatic Effect of Ambipolar Diffusion

We perform standard shearing-box MHD simulations for a local patch of a PPD at a fixed radius of $R = 1$ AU. The angular velocity is Ω, and we use isothermal equation state with sound speed c_s. The disk is vertically stratified with pressure scale height $H = c_s/\Omega$. We initiate the simulation with a Gaussian density profile (hydrostatic equilibrium) with midplane density ρ_0. Physically, we adopt the minimum-mass solar nebular disk model (MMSN, Weidenschilling, 1977), while in code unit, we set $c_s = \Omega = H = \rho_0 = 1$. The effect of cosmic-ray ionization, X-ray ionization are included as described in Bai (2011a), where the ionization rates are given as a function of horizontally averaged column density to the disk surface (which we evaluate in real simulation time). The magnetic diffusion coefficients for Ohmic resistivity and AD are interpolated from a lookup table based on the local density and ionization rate assuming equilibrium chemistry (Bai, 2011a,b). We use outflow vertical boundaries with zero gradient on gas velocity and magnetic fields and gas density is extrapolated assuming hydrostatic equilibrium.

We start by performing two three-dimensional (3D) simulations. In both runs, we adopt an initial magnetic field configuration as pure vertical, with its field strength characterized by $\beta_0 = 10^5$, where β_0 is the ratio of midplane gas pressure to magnetic pressure. Note that the net vertical field is a conserved quantity in shearing-box simulations. The simulation box size is $4H \times 8H \times 16H$ in the radial (x), azimuthal (y) and vertical (z)

https://doi.org/10.1017/S1743921313012933 Published online by Cambridge University Press

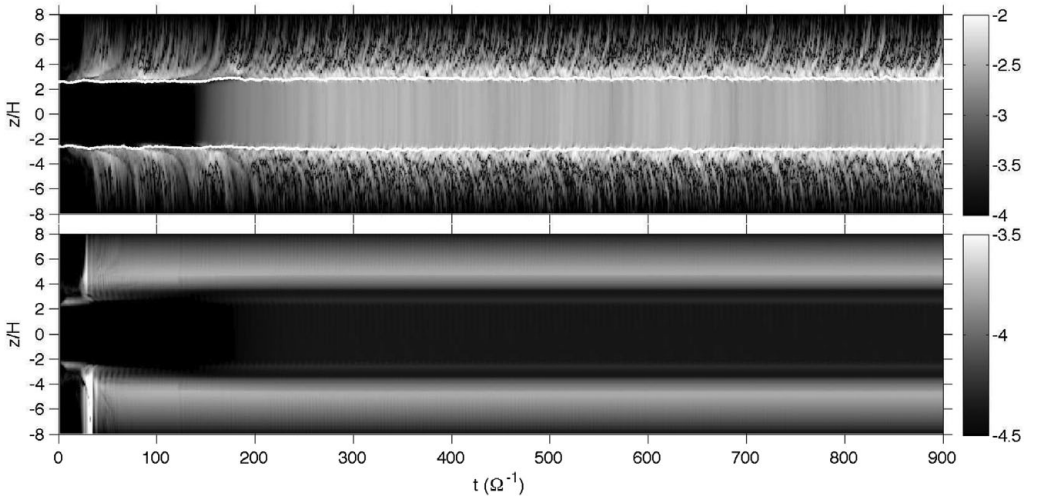

Figure 1. Time evolution of horizontally averaged vertical profiles of the Maxwell stress in the two fiducial runs. Top: simulation where only Ohmic resistivity is included. Bottom: simulation where both Ohmic resistivity and AD are included. Colors are in logarithmic scales. White contours in the upper panel correspond to the vertical Elsasser number $\Lambda_z \equiv v_{Az}^2/\eta_O\Omega = 1$.

dimensions. In the first run, only Ohmic resistivity is included, a situation that has been extensively adopted in the literature. In the second run, both Ohmic resistivity and AD are included, which is the first time that both effects are included in PPD simulations. Both simulations are run for about 150 orbits ($900\Omega^{-1}$). The main diagnostics adopted here are the $r\phi$ components of the Maxwell and Reynolds stress tensors, defined as

$$T_{r\phi}^{\rm Max} \equiv -\overline{B_x B_y}\ , \qquad T_{r\phi}^{\rm Rey} \equiv \overline{\rho v_x v_y'}\ , \tag{2.1}$$

where the overline denotes horizontal average, v_y' is the azimuthal velocity with Keplerian velocity subtracted, and the system has magnetic permeability $\mu = 1$.

In Figure 1 we show the evolution of the vertical Maxwell stress profile for both runs. In the Ohmic-resistivity-only case, very vigorous turbulence develops in the surface layer of the disk, characterized by strong and highly fluctuating Maxwell stress. The midplane region, while also possesses relatively large stress, has very little time variations. This is the conventional picture of layered accretion, and the midplane region corresponds to the "undead zone" (Turner & Sano, 2008). When AD is also included, we see that although the initial field configuration is unstable to the MRI, which grows and amplifies the magnetic field in the beginning, the system then quickly relaxes to a completely laminar state where the field lines are ordered and the system behaves essentially as in 1D. The reason for the suppression of the MRI is that the surface region is in the AD dominated regime where weak field is required for the MRI to operate, while the magnetic field is over-amplified by the initial growth of the MRI, which quenches itself.

3. Nature of the Laminar Wind Solution

We focus on the newly obtained 1D laminar solution and examine its properties. In Figure 2, we plot the poloidal field geometry of the solution, together with the velocity vectors. We see that the laminar solution corresponds to a disk outflow: the magnetic field is sufficiently bent beyond $z \sim 4.5H$ and the magnetocentrifugal mechanism accelerates the outflow beyond Alfvén speed as the gas escapes from vertical boundaries.

https://doi.org/10.1017/S1743921313012933 Published online by Cambridge University Press

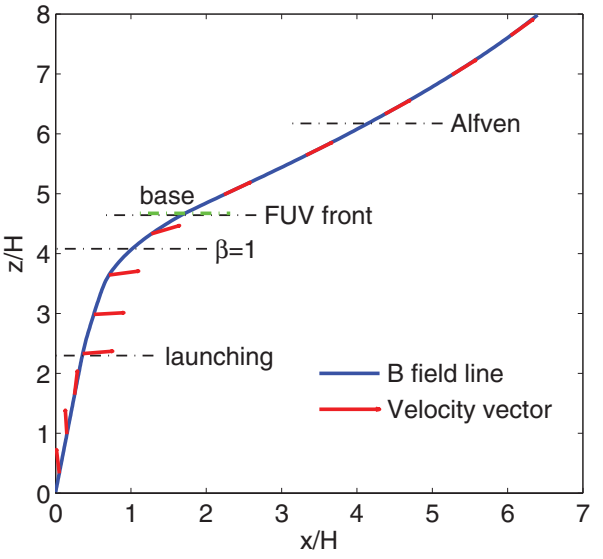

Figure 2. The poloidal field line geometry in our laminar wind solution (blue solid line). Overplotted are the unit vectors of the poloidal gas velocity (red arrows). The location of the wind launching point, the plasma $\beta = 1$ point, the FUV ionization front and the Alfvén point are indicated (black dash-dotted). Also marked is the location at base of the wind (green dashed).

In Figure 3 we further show the vertical profiles of magnetic fields and velocities in solid lines. Near the disk midplane, the magnetic fields are gas are essentially decoupled due to excessively large resistivity. As a result, magnetic field lines are straight, and are predominantly toroidal. Beyond $z \sim 2.3H$ (marked as the "launching" point), Ohmic resistivity is sufficiently reduced so that gas becomes partially coupled to the magnetic field, and the dominant non-ideal MHD effect is switched to AD. In this region, there is a large vertical gradient of the toroidal magnetic field. This gradient drives a radial current, which gives rise to Lorentz force in the toroidal direction, and has to be balanced by the Coriolis force. This explains the outward radial velocity of the gas between $z = 2.3 - 4.5H$. The outward motion of gas bends the magnetic field via ion-neutral drag, which is essential for the poloidal field to achieve relatively large bending angle and wind launching via the magnetocentrifugal mechanism. The flow becomes magnetically dominated at around $z \sim 4.1H$, beyond which the gas has limited influence on the magnetic fields and field lines become straight again. Finally, at the base of the wind, where the azimuthal velocity becomes super-Keplerian, the wind is launched and constantly accelerated magnetocentrifugally. Also marked in Figure 2 is the location of the far-UV (FUV) ionization front, beyond which the FUV ionization makes the gas sufficiently ionized (in the inner disk) and behave as in the ideal MHD regime. Correspondingly, the flow streamlines are aligned with magnetic field lines within the FUV layer. Below the FUV ionization front, poloidal gas velocity deviates from poloidal field lines due to AD.

We divide the vertical structure of the wind solution into the disk zone and the wind zone, separated at the base of the wind $z = \pm z_b$ discussed before, and in our fiducial simulation $z_b \approx 4.7H$. The rate of angular momentum transport carried by the wind is characterized by the $z\phi$ component of the stress tensor at the base of the wind

$$T^{\rm Max}_{z\phi}\Big|_{z=\pm z_b} \equiv -\overline{B_z B_y}\Big|_{z=\pm z_b}\ , \qquad T^{\rm Rey}_{z\phi}\Big|_{z=\pm z_b} \equiv \overline{\rho v_z v'_y}\Big|_{z=\pm z_b} = 0\ . \tag{3.1}$$

https://doi.org/10.1017/S1743921313012933 Published online by Cambridge University Press

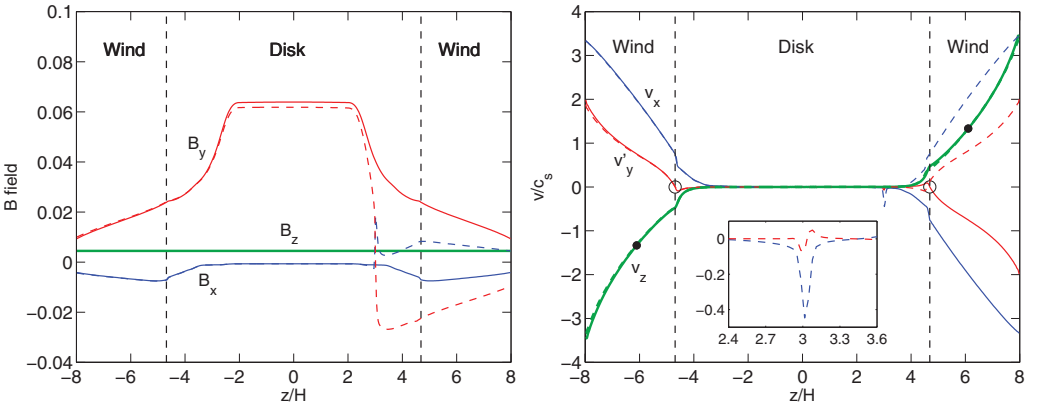

Figure 3. The vertical profiles of magnetic fields (left) and velocities (right) in the laminar wind solution. Solid lines correspond to the solution obtained from our fiducial 3D simulations, where the outflow symmetry is inconsistent with a global wind. Big black dots mark the Alfvén points, and open circles mark the base of the wind, where toroidal velocity becomes super-Keplerian. Dashed lines show an additional simulation where the outflow geometry is physical for a global wind. The inset on the right panel shows the zoomed-in view of the horizontal velocity profiles at the strong current layer. This is essentially how accretion proceeds in the wind-driven scenario.

Note that the Reynolds component is by definition zero at the base of the wind since $v_y'|_{\pm z_b} = 0$. The wind-driven accretion rate is then given by

$$\dot{M} = \frac{4\pi}{\Omega} R T_{z\phi}^{\rm Max}\Big|_{-z_b}^{z_b} \approx 4.1\times10^{-8} M_\odot \ {\rm yr}^{-1} \left(\frac{|T_{z\phi}^{\rm Max}|}{10^{-4}\rho_0 c_s^2}\right) R_{\rm AU}^{-3/4} \ , \tag{3.2}$$

where we have adopted the MMSN disk model to derive the numbers. We find from our laminar wind solution that $\left|T_{z\phi}^{\rm Max}\right|_{z=\pm z_b} \approx 1.1\times10^{-4}\rho_0 c_s^2$. This means that even with a very weak net vertical magnetic flux ($\beta_0 = 10^5$), the magnetocentrifugal wind launched from the disk can easily account for the typical observed accretion rates in PPDs.

In the laminar wind solution from our 3D simulation, the profiles for the three magnetic field components are all symmetric about the disk midplane. This field geometry is problematic because the outflows from the top and bottom sides of the disk point toward opposite directions, while in reality they should point toward the same direction (away from the star). In fact, the unphysical field geometry does not lead to net angular momentum transport since $T_{z\phi}$ at the two sides of the disk have the same sign and cancel out. Therefore, it is essential to seek for alternative solution with physical wind geometry.

We note that since curvature is neglected in the shearing-box approximation, the "inner" and "outer" sides of the box are completely symmetric, hence the direction that field lines bend is random. The randomness applies to both the top and bottom sides of the disk, and they behave independently. Therefore, by changing the random seed perturbation in our simulations, we have about 50% of chance to achieve a solution with a physical wind geometry. In Figure 3, we further show the profiles of magnetic fields and velocities for the physical wind solution in dashed lines. We see that the solution is almost exactly the same as the previous unphysical solution, except that the horizontal magnetic fields are flipped at about $z \sim 3H$. The flip leads to a strong current layer, which is also reflected in the velocity profile (see the inset). There is a rapid inflow with velocity of the order $0.3c_s$ at the strong current layer. In fact, this is how accretion proceeds: essentially all the stress $T_{z\phi}$ is exerted to the strong current layer, which forces the gas in this thin layer to drift inward, while the rest of the gas in the disk is almost static.

https://doi.org/10.1017/S1743921313012933 Published online by Cambridge University Press

Although the fraction of mass involved in the strong current layer is tiny ($\sim 5 \times 10^{-4}$), the large radial drift velocity makes it sufficient to carry the entire accretion flow.

We finally note that the strong current layer is offset from the midplane. This is again because the midplane region is too resistive where gas and magnetic field become decoupled and does not support current.

4. Discussion and Implications

By exploring different field configurations and other parameters, we find that necessary conditions for wind launching include: 1). Ohmic resistivity dominated midplane region; 2). AD dominated disk surface; 3). Presence of net vertical magnetic flux; and 4). Strong FUV ionization. Condition (2) always applies in PPDs, conditions (1) and (4) applies only to the inner region of PPDs. While there is no proof for condition (3), it is very unnatural for PPDs to possess absolutely zero net poloidal flux. Moreover, our study suggests that the presence of net poloidal flux is essential for driving rapid accretion. In sum, we conclude that the laminar accretion scenario applies in the inner region of PPDs at least in the vicinity of 1 AU.

We note that the location of 1 AU and its vicinity lies the habitable zone for solar-type stars. The fact that this region is completely laminar makes it the most favorable spot for grain growth, settling and planetesimal formation. Our results also has strong implications on the global evolution of PPDs, and we stress that global disk evolution is interconnected with magnetic flux distribution. Their mutual dependence can only be addressed in global simulations. Finally, while our work demonstrates the dramatic effect of AD in PPDs, the Hall effect is still not included in our study, which also plays a significant role in PPDs. This is planned for future work.

References

Bai, X.-N. 2011a, *ApJ*, 739, 50
Bai, X.-N. 2011b, *ApJ*, 739, 51
Bai, X.-N. & Goodman, J. 2009, *ApJ*, 701, 737
Bai, X.-N. & Stone, J. M. 2011, *ApJ*, 736, 144
Balbus, S. A. & Hawley, J. F. 1991, *ApJ*, 376, 214
Blandford, R. D. & Payne, D. G. 1982, *MNRAS*, 199, 883
Combet, C. & Ferreira, J. 2008, *A&A*, 479, 481
Ferreira, J. & Pelletier, G. 1995, *A&A*, 295, 807
Fleming, T. & Stone, J. M. 2003, *ApJ*, 585, 908
Hartigan, P., Edwards, S., & Ghandour, L. 1995, *ApJ*, 452, 736
Hartmann, L., Calvet, N., Gullbring, E., & D'Alessio, P. 1998, *ApJ*, 495, 385
Ilgner, M. & Nelson, R. P. 2006, *A&A*, 445, 205
Königl, A., Salmeron, R., & Wardle, M. 2010, *MNRAS*, 401, 479
Kunz, M. W. & Balbus, S. A. 2004, *MNRAS*, 348, 355
Okuzumi, S. & Hirose, S. 2011, *ApJ*, 742, 65
Pandey, B. P. & Wardle, M. 2012, *MNRAS*, 423, 222
Perez-Becker, D. & Chiang, E. 2011, *ApJ*, 735, 8
Sano, T. & Stone, J. M. 2002, *ApJ*, 577, 534
Turner, N. J. & Sano, T. 2008, *ApJ* Letter, 679, L131
Wardle, M. & Koenigl, A. 1993, *ApJ*, 410, 218
Weidenschilling, S. J. 1977, *Ap&SS*, 51, 153

https://doi.org/10.1017/S1743921313012933 Published online by Cambridge University Press